

1 **Mapping global onshore wind turbines using multi-source remote**  
2 **sensing images and hybrid learning approaches**

3 Shujun Li<sup>1,6</sup>, Jianchuan Qi<sup>2,3,4,\*</sup>, Yongze Song<sup>5</sup>, Peng Wang<sup>1,6,\*</sup>

4

5 1. State Key Laboratory for Ecological Security of Regions and Cities, Institute of  
6 Urban Environment, Chinese Academy of Sciences, Xiamen, Fujian 361021, China

7 2. School of Environment, Tsinghua University, Beijing, 100084, China

8 3. Institute for Carbon Neutrality, Tsinghua University, Beijing, 100084, China

9 4. TianGong Think Tank, Research Institute for Environmental Innovation (Suzhou)  
10 Tsinghua, 215163, China

11 5. School of Design and the Built Environment, Curtin University, Perth, Australia

12 6. University of Chinese Academy of Sciences, Beijing, 100049, China

13

14 \* To whom correspondence may be addressed.

15 *Correspondence to:* [pwang@iue.ac.cn](mailto:pwang@iue.ac.cn), [jcqi@tsinghua.edu.cn](mailto:jcqi@tsinghua.edu.cn)

16

17

18

19

20

21

22

23

24

25

26

27

28

29

30

31

32

33 **Abstract.** Wind power serves as a vital zero-carbon alternative to fossil fuels for  
34 climate change mitigation. Nevertheless, the vast expansion of wind turbine installation  
35 requires extensive terrestrial resources, raising wide concerns regarding land use  
36 competition and ecological impacts. Quantifying these effects necessitates near real-  
37 time geospatial data on wind turbine placement and density. However, current methods  
38 remain inadequate ~~monitoring for~~ for monitoring the fast-growing wind turbine  
39 deployment. Here, we developed an integrated framework that combines  
40 OpenStreetMap (OSM) data with multi-source remote sensing images (Google Earth  
41 and Sentinel-1/2) and deep learning and traditional machine learning models (ResNet-  
42 18 and Random Forest) to map global onshore wind turbines. Our models achieve  
43 validation accuracy >97% while enabling cost-effective, timely updates of global  
44 onshore wind turbines. Eventually, we established a geographical dataset  
45 (GonshoreWT2024) covering a total of 416,532,379,595 wind turbines globally by 2024.  
46 This dataset represents a tenfold expansion over ~~currently available~~ global wind turbine  
47 inventories as of 2020, and updates 42,955 more onshore wind turbines compared to  
48 the Global Renewables Watch based on lower computational requirements. In addition,  
49 we found that 80.87% wind turbines are situated on cropland and grassland, followed  
50 by forest and bare ground. This dataset facilitates essential studies on renewable energy  
51 land management, ecological impact analysis, and data-driven energy transition  
52 policies. The codes and dataset of the global onshore wind turbines ~~is~~ are available at  
53 the Zenodo link:  
54 <https://doi.org/10.5281/zenodo.18984175><https://doi.org/10.5281/zenodo.17217523>  
55 (Shujun et al., 2025).

## 57 **1 Introduction**

58 Wind energy will increase substantially over the coming decades to meet clean energy  
59 targets (Mckenna et al., 2025). Under the 1.5°C scenario, global installed wind power  
60 capacity is projected to reach nearly 10,300 GW by 2050, with onshore wind  
61 comprising 75% of total installations (Raimi et al., 2023). Compared to other energy  
62 technologies, wind power exhibits relatively low land use efficiency when accounting  
63 for wind turbine spacing requirements (Dai et al., 2024). Accordingly, meeting future  
64 deployment targets will necessitate substantial land allocations, raising pressing  
65 concerns about land-use conversion and biodiversity loss that demand urgent attention  
66 (Kati et al., 2021; Rinne et al., 2018). However, detailed geospatial data at the facility  
67 level is particularly required for the quantification of these impacts (Kruitwagen et al.,  
68 2021).

69 Indeed, asset-level data and facility arrangement are essential for power generation  
70 nowcasting and forecasting, as well as for decision-making by grid operators and  
71 energy stakeholders (Calvert et al., 2013; Tavakkoli et al., 2021). For instance,  
72 geospatial analysis of historical placements can inform wind turbine siting decisions by  
73 revealing both human and environmental landscape factors (Roddis et al., 2018).  
74 Previous research confirmed that substantial positional errors exist in the current

75 available wind facility records, especially pronounced in high-growth renewable energy  
76 markets (Cerri et al., 2024; Effenberger and Ludwig, 2022). A timely geospatial data  
77 set is critically needed to maintain accurate records of wind energy infrastructure, given  
78 its unprecedented growth rate. The dataset could also support data-driven metrics for  
79 Sustainable Development Goals (SDGs) (Mishra et al., 2024), including SDG 7  
80 (Affordable and Clean Energy), SDG 13 (Climate Action), and SDG 15 (Life on Land).

81 Despite the demonstrated importance of location data, only a few spatially explicit  
82 datasets are publicly available. At the global scale, ~~there is~~ a geospatial wind turbine  
83 dataset for 2020 is introduced (Dunnett et al., 2020), but its update mechanism depends  
84 entirely on OpenStreetMap (OSM), a crowdsourced data derived from heterogeneous  
85 contributors that could introduce significant uncertainty. Meanwhile, while multiple  
86 frameworks exist for updating global offshore wind turbine data (Hoeser et al., 2022;  
87 Zhang et al., 2021), onshore wind turbine updating methods remain underdeveloped  
88 due to their greater spatial distribution and environmental variability. Recently,  
89 Microsoft and Planet's Global Renewables Watch platform employs deep learning for  
90 global wind and solar monitoring (Robinson et al., 2025), but it demands massive  
91 computing resources ~~for data updates and provides only web-based queries without~~  
92 ~~editable datasets~~. At the national level, there are geospatial datasets for the United States  
93 (Rand et al., 2020), Germany (Manske et al., 2022), ~~and~~ Italy (Smeraldo et al., 2020),  
94 and South Africa (Kleebauer et al., 2025). However, inconsistent data collection ~~method~~  
95 methods across datasets with delays in update frequencies could hinder their systematic  
96 comparability. Currently, the research community lacks both a unified methodology and  
97 accessible datasets for tracking worldwide onshore wind turbine deployments.

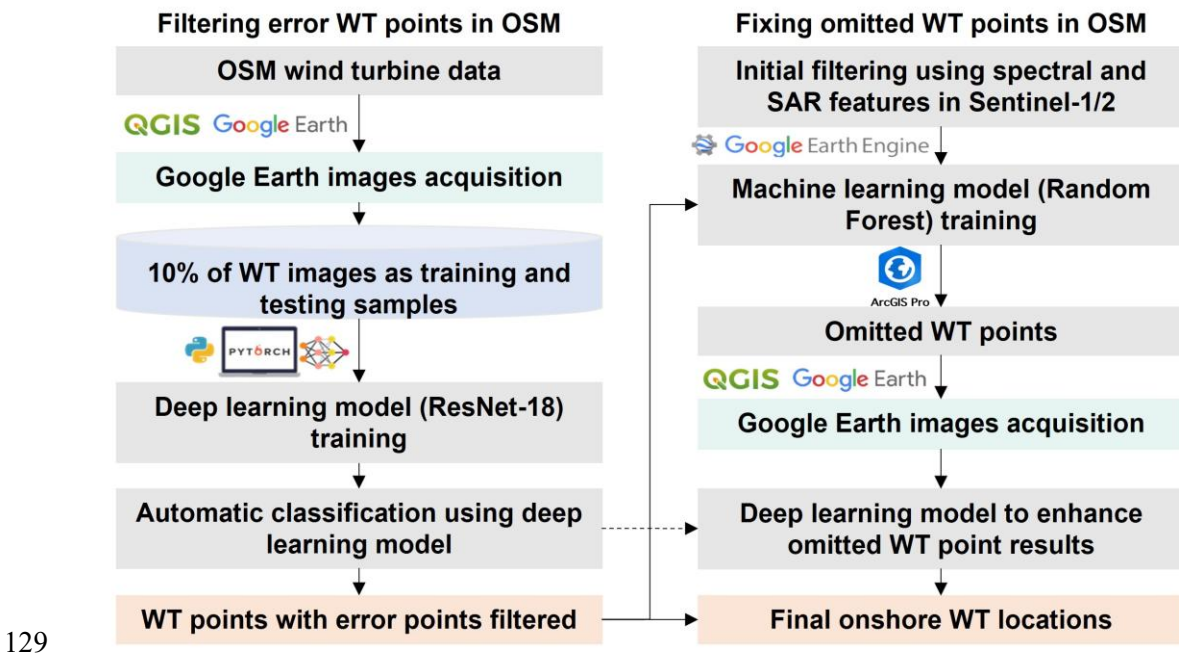
98 To address these gaps, our study presents a hybrid framework combining deep learning  
99 and a traditional machine learning framework for updating global onshore wind turbine  
100 data. By integrating multi-source remote sensing data (Google Earth high-resolution  
101 images, Sentinel-1, and Sentinel-2), our workflow systematically detects and validates  
102 global onshore wind turbines to generate a 2024 geodatabase (GonshoreWT2024). With  
103 OSM wind turbine locations as initial inputs, the two-stage locating process involves:  
104 (1) training a deep learning classifier (ResNet-18) on Google high-resolution images to  
105 identify and correct erroneous OSM records, followed by (2) detecting omitted wind  
106 turbines with Sentinel-1/2 spectral features and a Random Forest model trained on  
107 Google Earth Engine (GEE). Additionally, we examined worldwide land use  
108 characteristics of wind turbine sites and their national distribution patterns to assess  
109 current wind energy spatial utilization. Our study delivers comprehensive monitoring  
110 tools and datasets essential for tracking wind energy growth, enabling data-driven  
111 policy decisions to advance sustainable wind power development worldwide.

112

113 **2 Materials and methods**

114 **2.1 Framework**

115 The proposed framework combines OSM's crowdsourced geospatial data with a two-  
116 stage deep learning/traditional machine learning pipeline (**Figure 1**) to locate a  
117 ~~comprehensive~~ global onshore wind turbine ~~location~~ dataset for 2024. The first part  
118 involves utilizing OSM wind turbine coordinates to extract high-resolution Google  
119 Earth images, then training a ResNet-18 convolutional neural network to classify and  
120 flag erroneous wind turbines in the OSM dataset. The second part employs confirmed  
121 wind turbine locations to train a Random Forest classifier for potential omitted wind  
122 turbines using Sentinel-1/2 features at GEE, ~~combining~~ combining with validation  
123 through our pre-trained ResNet-18 model applied to Google high-resolution images of  
124 the potential points. The integrated output merges error-corrected OSM data with  
125 supplemented wind turbine omissions, generating an enhanced global dataset that  
126 demonstrates improved spatial accuracy and comprehensive operational wind turbine  
127 coverage. This framework reduces barriers to entry by using publicly available  
128 platforms, offering a cost-saving and resource-efficient alternative.



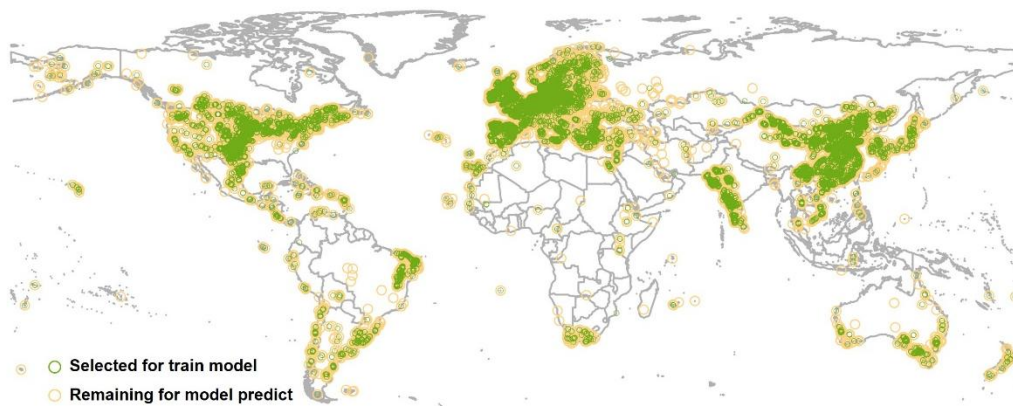
129  
130 **Figure 1.** Framework for mapping global onshore wind turbines. Where the WT  
131 represents wind turbines, OSM represents OpenStreetMap.

132 **2.2 Two-phase approach for global onshore wind turbine mapping**

133 **2.2.1 Filtering of erroneous data with deep learning model**

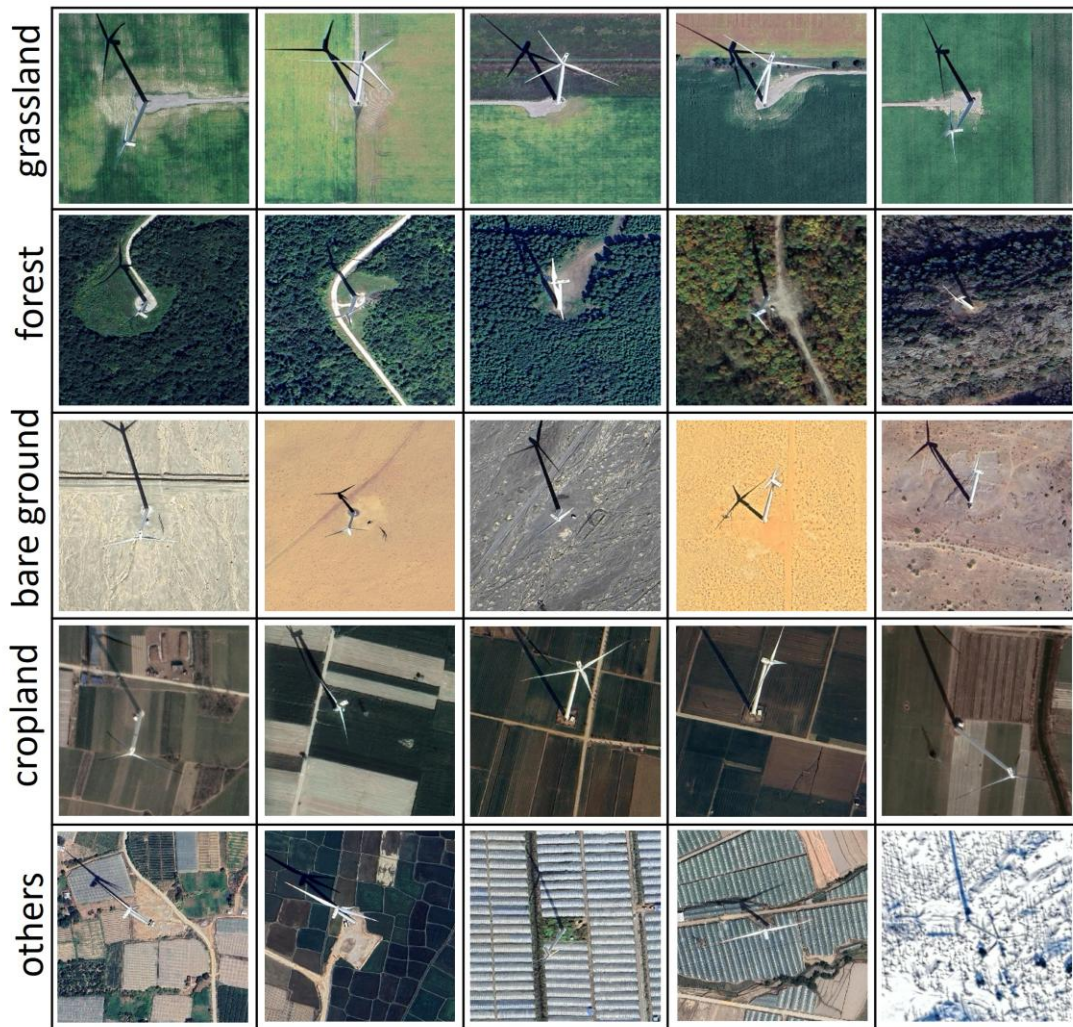
134 We obtained the baseline OSM 2024 wind turbine dataset through the QuickOSM  
135 plugin (based on the Overpass API) in QGIS software using the Overpass API plugin  
136 with the query parameter: generator: source=wind["generator: source="wind"].

137 Given our focus on the individual wind turbine level, we utilized this query filter for  
138 nodes representing wind turbines in the format of point features. Since we focus on  
139 onshore wind turbines, the OSM land polygon derived from  
140 <https://osmdata.openstreetmap.de/data/land-polygons.html> is used to define the study  
141 extent and refine the dataset. We refined the dataset by applying OSM land polygons  
142 (<https://osmdata.openstreetmap.de/data/land-polygons.html>), resulting in a  
143 preliminary global inventory of 377,154 geolocated onshore wind turbines with  
144 complete metadata records. Given OSM's crowdsourced feature due to unverified  
145 contributors, the extracted wind turbine locations serve as initial references that demand  
146 thorough validation. Subsequent analysis must systematically regarding addressing both  
147 commission errors (false positives) and omission errors (omitted wind turbines) through  
148 technical verification.



150 **Figure 2.** Spatial distribution of training samples (green points).

151 Based on the OSM-derived wind turbine coordinates, we ~~created~~ generated  
152 500m×500m extraction zones (~~QGIS Buffer Tool~~) to acquire high-resolution Google  
153 Earth images through the Buffer Tool in QGIS software. This conservative spatial  
154 buffer accounts for maximum wind turbine diameters ( $\leq 200\text{m}$ ) while guaranteeing full  
155 rotor coverage (Muller et al., 2024). The image tiles were resized to a standardized  
156 ~~256×256 pixel~~ 256-pixel format, maintaining optimal input dimensions for our ResNet-  
157 18 architecture while retaining essential wind turbine characteristics. For model  
158 construction, we employed a strategically sampled 10% subset (37,285 images) from  
159 the complete dataset, which ~~balancing~~ balances representativeness with computational  
160 constraints during training. The spatial distribution of sampled wind turbine points  
161 exhibits balanced representation across global regions in **Figure 2**, confirming our  
162 stratified random sampling approach effectively maintained geographic diversity. This  
163 subset was manually annotated with labels for 'wind turbines' and 'non-turbines'. The  
164 labeled data was then split into a training set (60%, 22,372 images) ~~and~~ a testing sets  
165 (20%, 7,457 images), and a validation sets (20%, 7,456 images) for our OSM error  
166 classification model. Representative samples of the buffered wind turbine images are  
167 displayed in **Figure 3**. The visual data reveal that wind turbines are distributed across  
168 diverse landscapes, including grasslands, bare land, cropland, and forests, with  
169 occasional installations near water bodies and built environments.



© Google Earth 2024

170

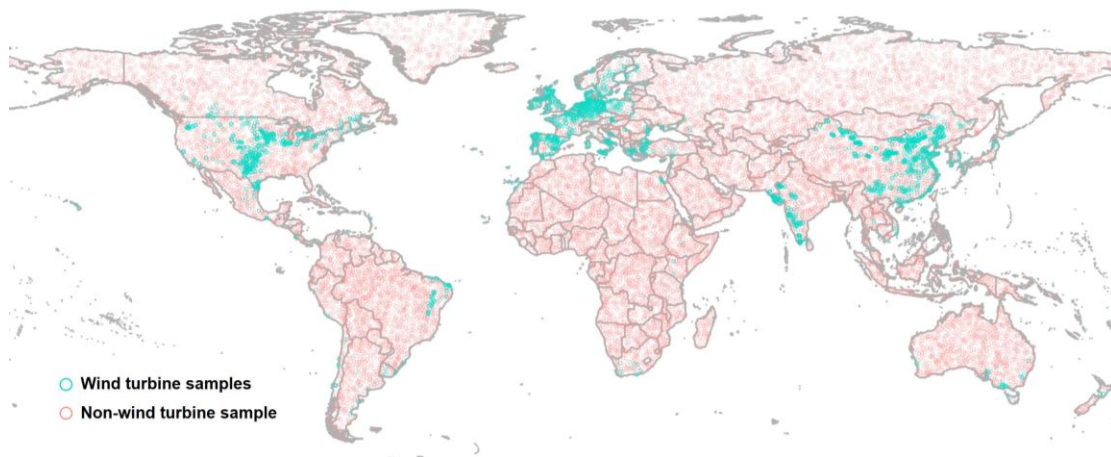
171 **Figure 3.** Different land types of onshore wind turbines in Google Earth images.

172 For automated classification of OSM wind turbine data, we employed the ResNet-18  
 173 architecture (He et al., 2016), leveraging its demonstrated image classification  
 174 capabilities while ensuring computational efficiency for geospatial applications at scale.  
 175 Our optimized ResNet-18 model processed all 339,869 candidate images, identifying  
 176 291,501 confirmed wind turbine locations (85.8% positive rate) while classifying  
 177 48,368 as non-turbine cases (14.2%). All negative classifications underwent rigorous  
 178 cross-platform verification using Google Earth, Bing Maps, and Sentinel-2 images,  
 179 enabling the removal of inaccurate OSM entries. These validated results were then  
 180 integrated with the training data to generate an enhanced global wind turbine dataset  
 181 with improved accuracy. The dataset and codes for training the model are available at  
 182 the Zenodo website:  
 183 <https://doi.org/10.5281/zenodo.18984175><https://doi.org/10.5281/zenodo.17217523>  
 184 (Shujun et al., 2025).

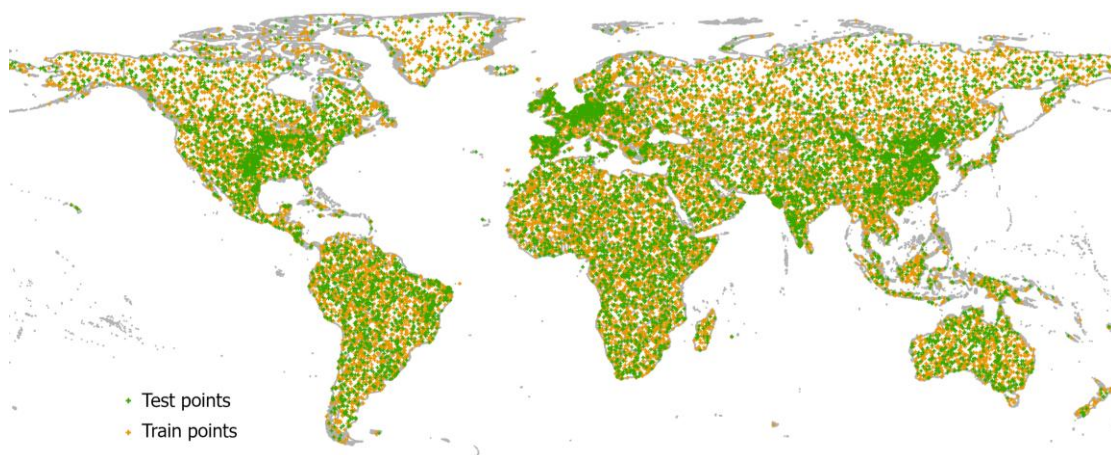
185 **2.2.2 Supplementing omitted data with traditional machine learning model**

186 Based on the deep learning-classified OSM wind turbine dataset and satellite images,

187 we developed an optimized Random Forest model for ~~comprehensive~~-omission  
188 detection (Rigatti, 2017). The Random Forest model was trained on GEE using verified  
189 wind turbine locations from OSM, alongside globally sampled negative samples  
190 **(Figure 4)**. We employ a global-scale uniform random sampling strategy. This ensured  
191 sufficient spatial separation and geographic diversity among samples, minimizing  
192 spatial dependency and maintaining sample independence. Besides, we apply a 30-  
193 meter buffer around all existing wind turbine locations (positive samples). These  
194 buffered areas are then masked out from the global sampling pool to ensure that no  
195 negative samples are drawn within this exclusion zone. Accordingly, we trained the  
196 Random Forest model with 10,000 globally distributed wind turbine locations (positive  
197 samples) and 20,000 non-turbine points (negative samples). The negative samples are  
198 obtained via globally uniform random sampling to ensure spatial objectivity. The  
199 resulting dataset encompasses diverse land-cover categories, including grasslands, bare  
200 land, cropland, and forests. ~~We trained the Random Forest model with 10,000~~  
201 ~~globally distributed wind turbine locations (positive samples) and 20,000 non-turbine~~  
202 ~~points (negative samples), and applied a 30m spatial buffer to negative samples to~~  
203 ~~ensure characteristic representation.~~The dataset was then split into 70% training and  
204 30% testing sets as illustrated in **Figure 54**.



206 **Figure 4.** Spatial distribution of wind turbine (positive) and non-turbine (negative)  
207 training samples for machine learning.

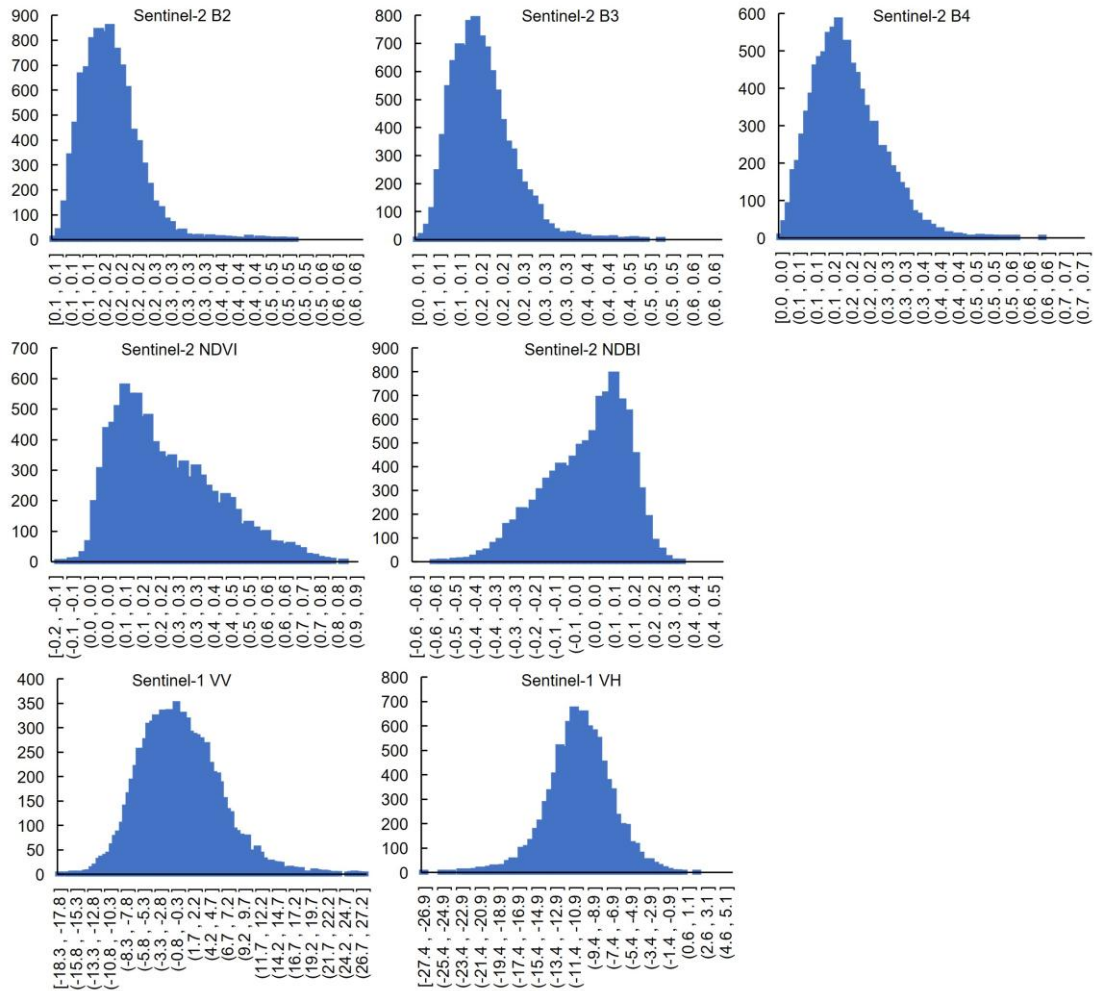


209 **Figure 45.** Spatial distribution of train and test datasets for the Random Forest model.  
210 The green ones represent the points selected for model training, and the orange ones  
211 represent the points selected for model testing.

212  
213 We constructed a comprehensive feature set for machine learning based on Sentinel-1  
214 and Sentinel-2 satellite imagery integrated via the GEE platform. We utilized the  
215 Sentinel-1 Ground Range Detected (GRD) dataset (COPERNICUS/S1\_GRD),  
216 extracting the VV and VH polarization bands. We employed the Sentinel-2 Surface  
217 Reflectance collection (COPERNICUS/S2\_SR\_HARMONIZED), which includes the  
218 visible and near-infrared (NIR) bands. To ensure data quality, we applied the QA60  
219 band for cloud masking in Sentinel-2 images. Both datasets were processed using a  
220 median reducer across the entire year of 2024 to generate cloud-free, representative  
221 composites. All spectral bands and backscatter coefficients were then normalized to a  
222 range of [0, 1] to mitigate effects from illumination conditions and sensor  
223 characteristics. Finally, these processed layers were stacked into a unified feature  
224 collection to serve as input for the machine learning models.

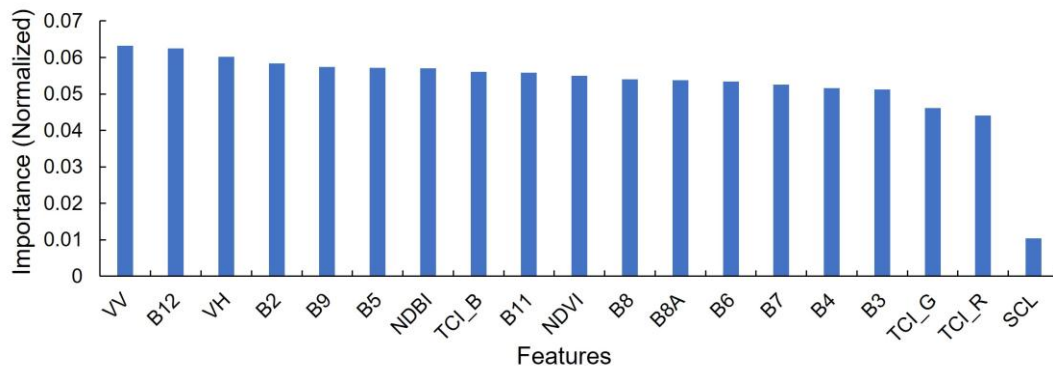
225 In addition to the original ~~spectral~~ bands from Sentinel-1 and Sentinel-2, we  
226 incorporated the Normalized Difference Vegetation Index (NDVI) (Huang et al., 2021)  
227 and the Normalized Difference Built-up Index (NDBI) (Zha et al., 2003) to enhance the  
228 differentiation between wind turbines and their background features based on the  
229 original bands from Sentinel-2. For comprehensive feature characterization, we  
230 implemented a random sampling strategy across 10,000 wind turbine locations, while  
231 covering all major wind development regions for reliable spectral analysis. **Figure 5-6**  
232 presents seven selected spectral feature value ~~distribution-distributions~~  
233 revealing distinct characteristic ranges for turbine signatures across different sensor  
234 bands. This demonstrates the effectiveness of different band features in wind turbine  
235 classification. To reduce the computational load of the Random Forest model, we  
236 excluded the 800-m buffer area of already validated wind turbines and then defined  
237 upper and lower threshold boundaries to filter out non-turbine areas during the initial  
238 processing stage. These thresholds include Sentinel-2's B2 [0, 0.3], B3 [0, 0.3], B4 [0,  
239 0.3], NDVI [0, 0.7], NDBI [0, 0.7], and Sentinel-1's VV [-18, 18] and VH [-25, 1].

240 The final dataset incorporated 19-dimensional feature data for each sample point, which  
241 was utilized for training the model to detect omitted wind turbine points. Our feature  
242 importance ranking of the 19-dimensional feature space (**Figure 67**) revealed that  
243 Sentinel-1's VV and VH polarization bands are particularly effective for identifying the  
244 wind turbines. This could contribute to the band's high sensitivity to vertical metallic  
245 structures such as wind turbine towers, as these act as corner reflectors that generate  
246 distinct bright signatures in SAR imagery. The Sentinel-2's B12 and B2 bands also show  
247 a strong response to wind turbine structures, which enhances their contrast against  
248 natural backgrounds like vegetation, soil, and water.



250

251 **Figure 56.** Feature value distribution of randomly selected wind turbine samples.



252

253 **Figure 67.** Feature importance ranking for building a Random Forest classification  
254 model.

### 255 2.3 Classification accuracy assessment of models

256 We evaluated the performance of both deep learning and traditional machine learning  
257 models using standard classification metrics computed from confusion matrices,  
258 namely precision, recall, and F1-score, as shown in Eq. (1)-(3), as based on an

independent test and validation set (Congalton, 1991; Goutte and Gaussier, 2005)— to  
ensure the model's generalizability and avoid over-optimization on training data.  
 Producer's accuracy (recall) quantifies the proportion of actual wind turbine locations  
 correctly detected, while user's accuracy (precision) represents the fraction of predicted  
wind turbines that are true positives. Where, The precision equals the number of true  
 positives (TP) divided by the sum of true positives (TP) and false positives (FP). Where  
 the recall equals the number of true positives (TP) divided by the sum of true positives  
 (TP) and false negatives (FN). The F1-score harmonizes these metrics, providing  
 particularly valuable evaluation for imbalanced wind turbine detection scenarios where  
 background features significantly outnumber target objects.

$$Precision = \frac{TP}{TP + FP} \quad (1)$$

$$Recall = \frac{TP}{TP + FN} \quad (2)$$

$$F1 - score = 2 \times \frac{Precision \times Recall}{Precision + Recall} \quad (3)$$

Based on our updated wind turbine dataset, we evaluated the data accuracy and errors  
within the OSM wind turbine records. We calculated omission and commission errors  
using a spatial proximity analysis in ArcGIS Pro with a 30-meter tolerance buffer. We  
applied a 30-m buffer to our generated points and performed a spatial selection on the  
OSM reference points to calculate the omission error. And the OSM points not captured  
within these buffers were classified as omissions. Conversely, to calculate the  
commission error, we buffered the OSM points and identified our generated points that  
fell outside these zones. The respective error rates were derived by dividing the count  
of omitted or committed points by the total number of OSM wind turbines. Finally,  
these two rates were summed to provide a total error rate.

#### **2.4 Land use occupation analysis of onshore wind turbines**

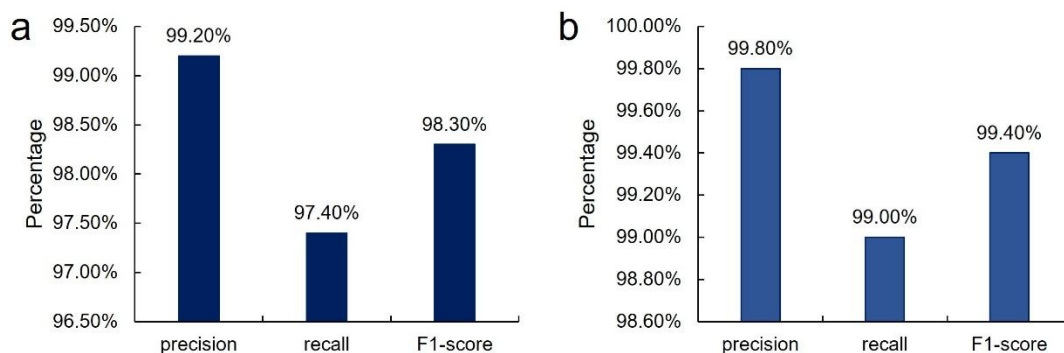
This study We utilizes ESRI's 2023 Land Use/Land Cover (LULC) dataset (Karra et al.,  
 2021), derived from ESA Sentinel-2 images at 10-meter resolution— for analyzing the  
 land use characteristics surrounding onshore wind turbines. The LULC composite maps  
 integrate annual predictions for nine defined categories, namely cropland, rangeland,  
 forest, built-up areas, bare ground, water bodies, flooded vegetation, snow/ice cover,  
 and cloud cover. By conducting spatial overlay analysis between our finalized global  
 onshore wind turbine dataset and the LULC classification within GEE, we  
 characterized land occupation patterns through the extraction of underlying land use

292 types at wind turbine sites. Additionally, we evaluated wind turbine land use impacts  
293 by conducting an 800-meter buffer ~~analyses~~ around wind turbine ~~locations~~ (Dunnnett et  
294 al., 2020), and converting the results to raster format for ~~comprehensive~~ spatial  
295 assessment.

## 296 3 Results

### 297 3.1 Evaluation results

298 **Figure 7a-8a** displays the deep learning model's performance for onshore wind turbine  
299 error filtering, achieving exceptional precision (99.2%), recall (97.4%), and F1-score  
300 (98.3%), respectively. The Random Forest model demonstrated equally strong  
301 performance, achieving 99.8% recall, 99.0% precision, and 99.4% F1-score (**Figure**  
302 **7b8b**). Importantly, the deep learning classifier achieved an 86% reduction in required  
303 manual verification (291,501 of 339,869 images). Meanwhile, our analysis revealed a  
304 ~~10~~18.5% error rate in OSM's global wind turbine dataset. The calculated discrepancy is  
305 yielded from the omission and commission error rates of 14.4% and 4.1%, respectively.  
306 It is worth noting that this error rate represents global averages, significant regional  
307 variations could exist as the OSM data fluctuates across different countries due to  
308 varying mapping efforts. While this validates its reliability for macro-scale trend  
309 analysis, the findings underscore inherent limitations of data directly obtained from  
310 OSM for precision-critical wind energy applications.



311  
312 **Figure 78.** Evaluation results of two models for wind turbine classification. **(a)** Precision, recall,  
313 and F1-score of the deep learning model. **(b)** Precision, recall, and F1-score of the traditional  
314 machine learning model.

### 316 3.2 Comparison with open-source datasets

317 To validate the accuracy of our wind turbine records, we cross-validated them against  
318 multiple authoritative geospatial datasets, including the 2020 global wind and solar  
319 dataset (Dunnnett et al., 2020), along with official and research-based wind turbine  
320 inventories from the United States (Rand et al., 2020), Italy (Smeraldo et al., 2020), ~~and~~  
321 Germany (Manske et al., 2022), and South Africa (Kleebauer et al., 2025). Our dataset  
322 (GonshoreWT2024)Our 2024 global inventory documents 416,532,379,595 wind

323 turbines (**Table 1**), representing a tenfold expansion from the 2020 baseline of 33,514  
 324 wind turbines. Our The wind turbine counts of ~~GonshoreWT2024~~ closely aligns  
 325 with Global Renewables Watch's 2024 total of ~~(375,197-375,000~~ wind turbines),  
 326 showing with a merely 1.29.9% variance. The consistency between our estimates and  
 327 official records for temporally comparable years is high, with discrepancies of less than  
 328 2.3% in the United States and less than 0.3% in South Africa. The consistency between  
 329 our United States estimates ~~(74,487 turbines) and official revealed records ~~(75,781~~~~  
 330 turbines, <1.8% discrepancy) \_also\_ This also provides strong validation of our  
 331 methodology's precision. Our cross-validation across multiple data sources and regions  
 332 reveals both remarkable consistency and a substantial quantity of previously  
 333 unrecorded wind turbine installations.

334 **Table 1.** Comparison of open-source datasets of ~~onshore~~ wind turbines with our results.

Scope	Time	Number	Ours (2024)
Dunnnett et al. (2020)	2020	33,514	<del>416,532</del> 379, 595
Global Renewables Watch (Robinson et al., 2025)	2024( <u>Quarter 2</u> )	<del>375,000</del> 19 7	<del>416,532</del> 379, 595
United States (Rand et al., 2020)	2024	75,781	<del>74,052</del> 74,52 3
Germany (Manske et al., 2022)	2021	28,156	<del>29,971</del> 28,53 0
Italy (Smeraldo et al., 2020)	2020	8,729	<del>10,591</del> 10,14 7
<u>South Africa</u> (Kleebauer et al., 2025)	<u>2025</u>	<u>1,487</u>	<u>1,483</u>

335  
 336 We further benchmark our dataset against the current global-scale wind turbine datasets,  
 337 including Dunnnett et al. (2020) and Global Renewables Watch (**Table 2**). Results show  
 338 that our dataset contains the largest number of identified onshore wind turbines while  
 339 maintaining nation-level coverage and land type classification compared to Dunnnett et  
 340 al. (2020). In terms of data records, the Global Renewables Watch is updated to the  
 341 second quarter of 2024 with 375,197 wind turbines and includes a limited number of  
 342 offshore wind turbines that are not comprehensively. Our dataset focuses on onshore  
 343 wind turbines and incorporates additional updates by the end of 2024. Methodologically,  
 344 the Global Renewables Watch requires massive training datasets and substantial  
 345 computational resource budget exceeding 650 V100 GPU hours to process around 14  
 346 terapixels of satellite imagery (Robinson et al., 2025). In contrast, our hybrid  
 347 framework utilizes medium-to-high resolution imagery to enable global-scale updates  
 348 with significantly lower computational demands. By leveraging publicly available  
 349 platforms, this framework lowers the barrier to entry through a cost-effective and  
 350 resource-efficient alternative.

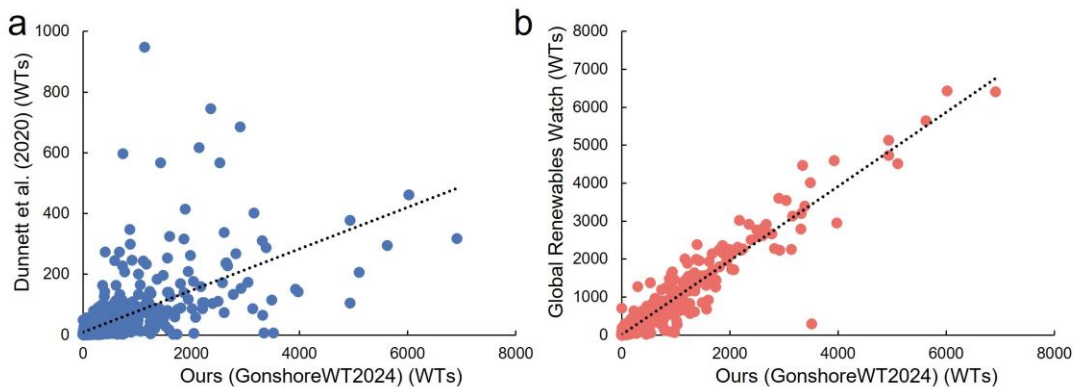
351 **Table 2.** Comparisons with current global-scale wind turbine datasets.

<u>Scope</u>	<u>Technology</u>	<u>Time</u>	<u>Number</u>	<u>Onshore number</u>	<u>Land type</u>	<u>Nation</u>	<u>Construction year</u>	<u>Updating algorithm</u>
<u>Dunnett et al. (2020)</u>	<u>Onshore and part Offshore</u>	<u>2020</u>	<u>33,514</u>	<u>33,240</u>	<u>No</u>	<u>Yes</u>	<u>No</u>	<u>No</u>
<u>Global Renewables Watch (Robinson et al., 2025)</u>	<u>Onshore and part Offshore</u>	<u>2024 (Quarter 2)</u>	<u>375,197</u>	<u>373,577</u>	<u>Yes</u>	<u>Yes</u>	<u>Yes</u>	<u>Yes</u>
<u>Ours (GonshoreWT2024)</u>	<u>Onshore</u>	<u>2024</u>	<u>416,532</u>	<u>416,532</u>	<u>Yes</u>	<u>Yes</u>	<u>No</u>	<u>Yes</u>

352

353 We also conducted a spatial distribution analysis to assess the correlation between our  
354 dataset and existing benchmarks, including the Dunnett et al. (2020) and Global  
355 Renewables Watch. Specifically, the global study area was partitioned into  $2^\circ \times 2^\circ$  grid  
356 cells to calculate wind turbine counts. We then employed scatter plots to evaluate the  
357 spatial consistency of our dataset relative to Dunnett et al. (2020) and the Global  
358 Renewables Watch (Figure 9). Subsequently, Pearson's  $r^2$  is calculated to quantify the  
359 correlation between the datasets. Our dataset shows a moderate correlation with  
360 Dunnett et al. (2020) (Figure 9a), with a Pearson's  $r^2$  of 0.4, primarily due to the  
361 significantly expanded coverage of our dataset. In contrast, our dataset shows a high  
362 correlation with Global Renewables Watch with a Pearson  $r^2$  of 0.93, indicating a high  
363 degree of geospatial consistency (Figure 9b).

364 Additionally, we quantified the mutual global underreporting between Global  
365 Renewables Watch and ours, which is around 20%. Global Renewables Watch has  
366 72,304 more different wind turbines than ours, and we have 80,532 more different wind  
367 turbines than theirs. We further conduct manual verification to quantify omission and  
368 commission rates of our dataset in these wind turbines. Final verification shows a 59%  
369 validity rate (43,011/72,304) for unique wind turbine entries of Global Renewables  
370 Watch, compared to a 92% validity rate (74,458/80,532) for ours. We further updated  
371 our dataset to a final global count of 416,532 wind turbines based on manual  
372 verification.



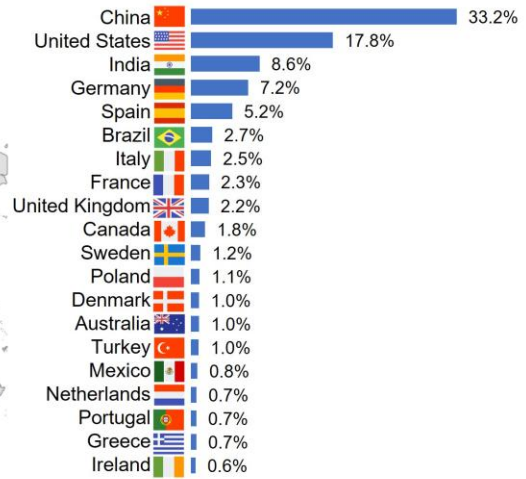
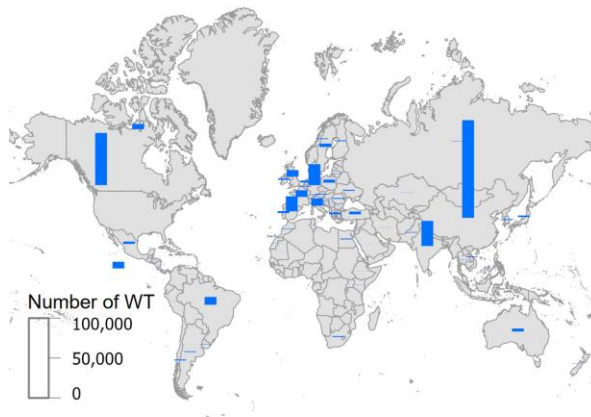
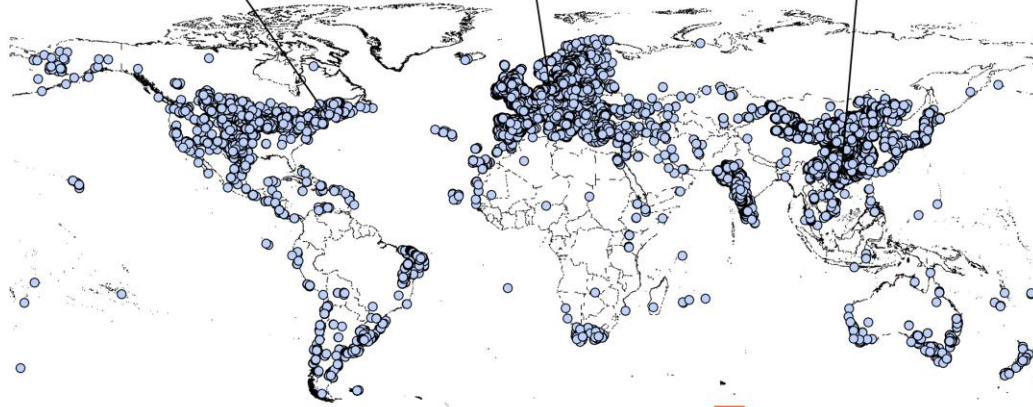
373

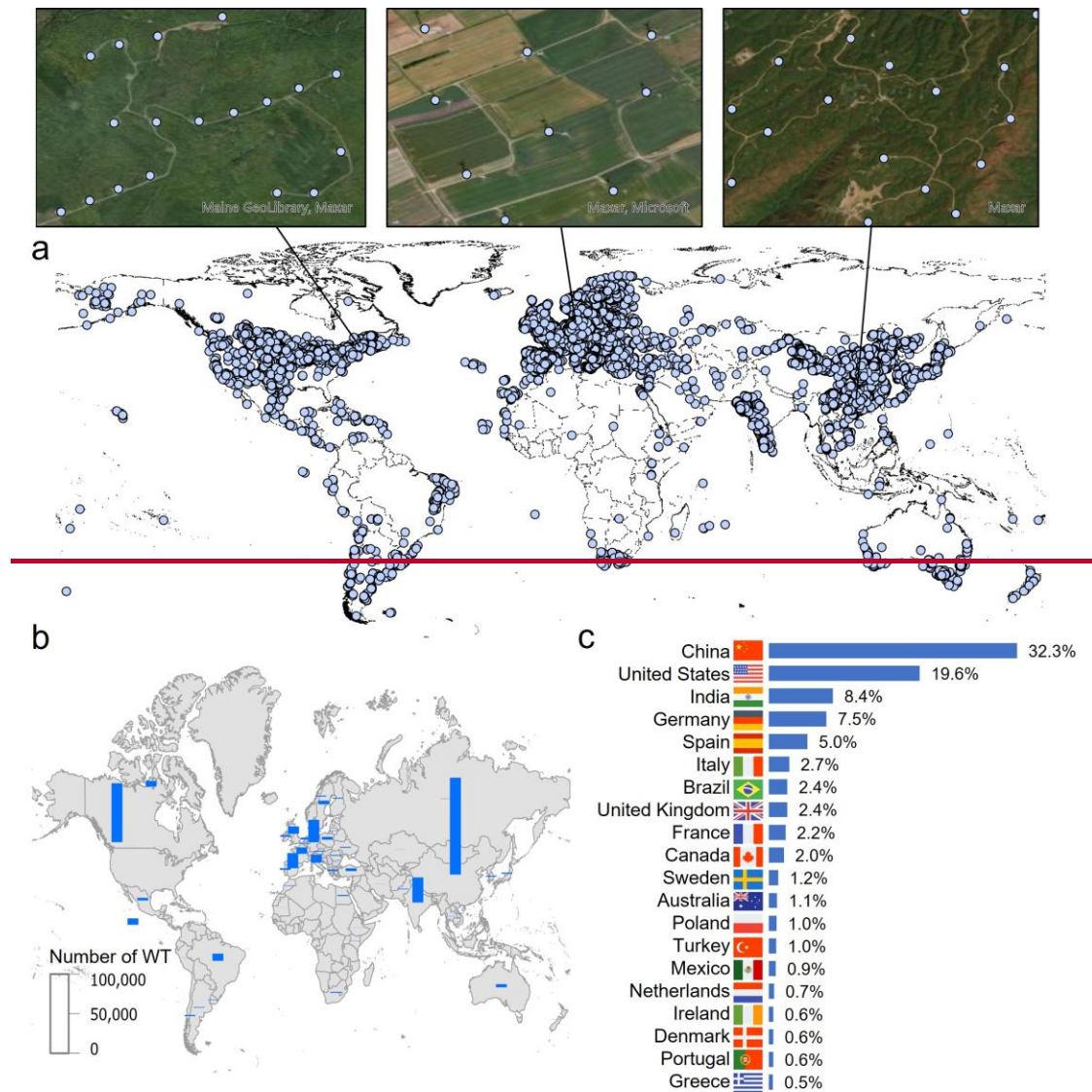
374 **Figure 9.** Global grid-based ( $2^\circ \times 2^\circ$ ) correlation analysis of our dataset (GonshoreWT2024)

375 and existing benchmarks. (a) Distribution of grid-level wind turbine counts between our dataset  
376 (GonshoreWT2024) and Dunnett et al. (2020). (b) Distribution of grid-level wind turbines  
377 between our dataset (GonshoreWT2024) and Global Renewables Watch.

### 378 **3.3 Global onshore wind turbine installation distribution**

379 The finalized global dataset (GonshoreWT2024) contains 416,532~~379,595~~ precisely  
380 georeferenced wind turbines (Figure 8a), exhibiting pronounced concentration ~~patterns~~  
381 across northern hemisphere regions (Figure 10a), particularly in North America,  
382 Europe, and East Asia. Regional deployment patterns also show clear geographic  
383 concentrations (Figure 8b10b). China dominates global wind energy  
384 deployment~~China's overwhelming dominance in global wind energy deployment~~, with  
385 138,486~~122,602~~ wind turbines representing 33.2~~32.3~~ % of worldwide installations. The  
386 United States ranks second (74,051~~74,523~~ wind turbines), followed by India  
387 (35,783~~31,736~~), Germany (29,970~~28,530~~), and Spain (21,543~~19,124~~), collectively  
388 representing the top five national markets (Figure 8e10c). China and India, collectively  
389 representing 89.75% of Asia's wind turbine installations, and the United States and  
390 Brazil together comprise 92.77% of American deployments. Europe's wind energy  
391 deployment is primarily concentrated in Germany, Spain, and Italy, which collectively  
392 account for 64.0% of global wind turbine~~European~~ installations.





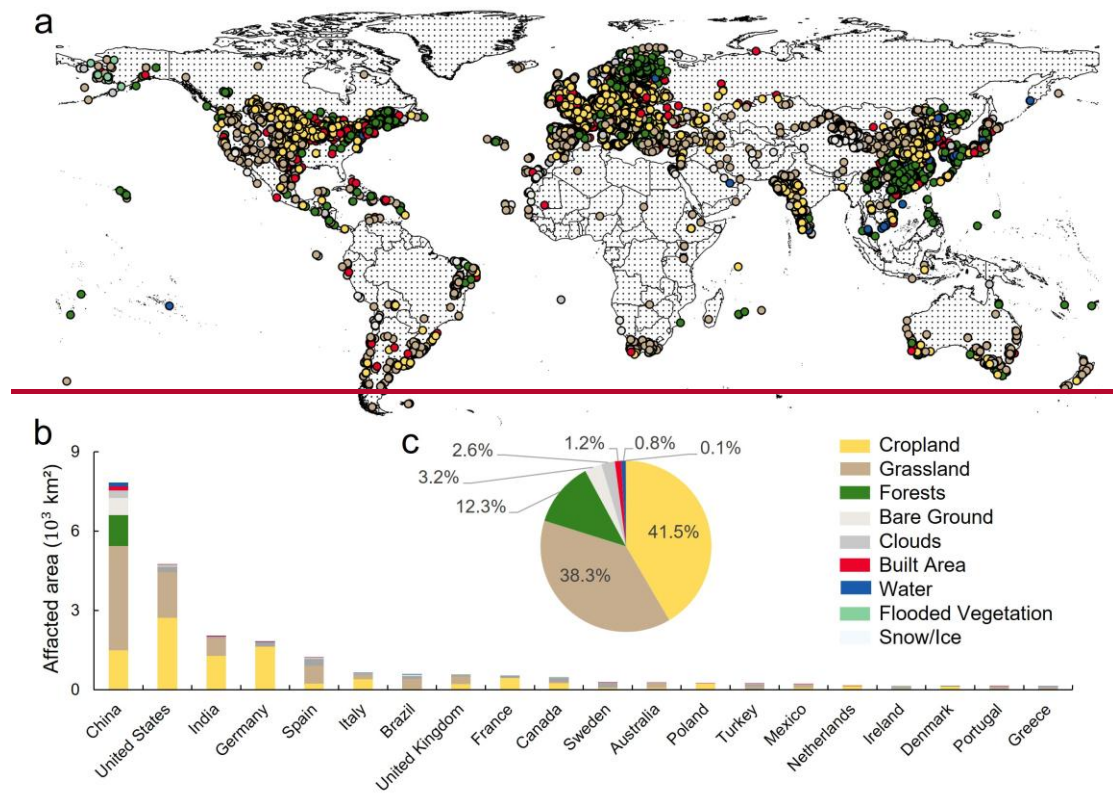
394

395 **Figure 810.** Global onshore wind turbine installation records and spatial distribution.  
 396 **(a)** Global onshore wind turbine by 2024. **(b)** Spatial distribution of wind turbine  
 397 installation statistics by country. **(c)** Percentage ranking of wind turbines for top 20  
 398 countries.

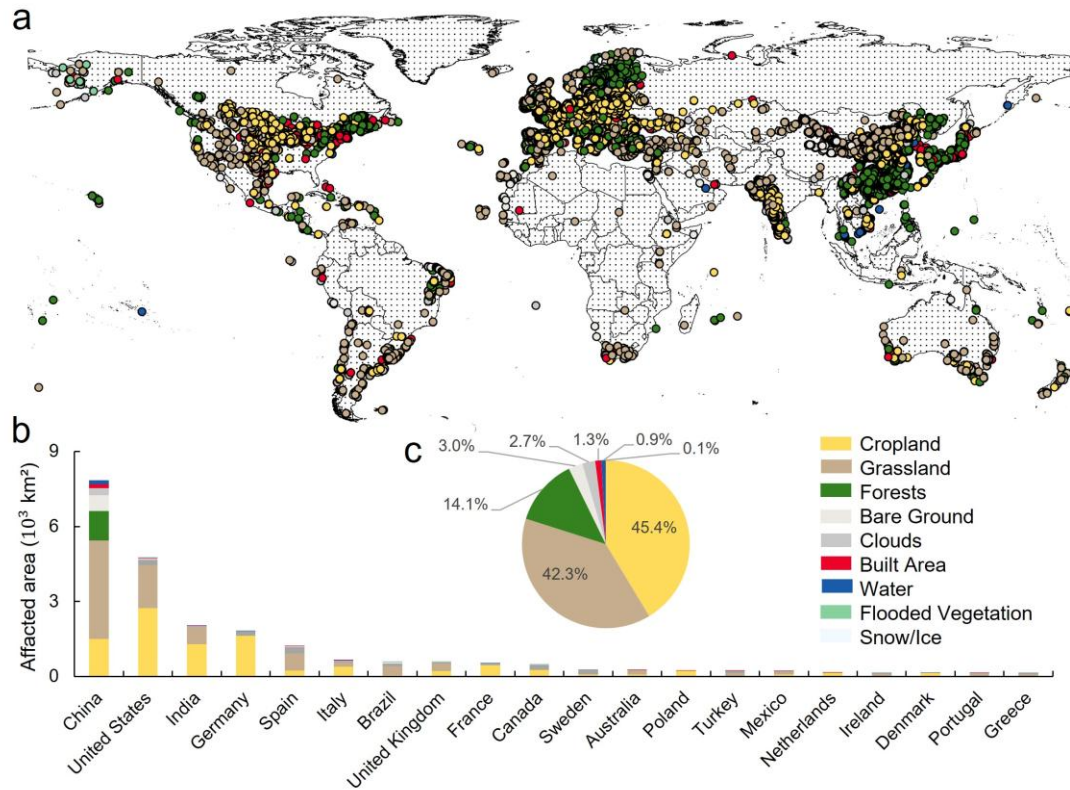
399 **3.4 Land use types and spatial distribution of global onshore wind turbines**

400 Our global assessment quantifies a total impacted area of 367,132,242,940 km<sup>2</sup> of the  
 401 wind turbines, which is estimated with an 800-meter buffer around wind turbine  
 402 locations (Dunnett et al., 2020). Among the affected areas, 8087% of wind turbines are  
 403 located within cropland and grassland ecosystems (**Figure 9e11c**). Specifically,  
 404 croplands represent the predominant land use at 4245% (165,209,400,915 km<sup>2</sup>),  
 405 followed by grasslands for 3842% (154,195,93,028 km<sup>2</sup>), and forests for 1214%  
 406 (51,398,29,832 km<sup>2</sup>). These proportions, however, exhibit substantial variation across  
 407 national boundaries (**Figure 9a11a, b**). China, the global leader in wind capacity,  
 408 exhibits unique siting patterns with over 50% of wind turbines deployed in grasslands,

409 followed by croplands (20%) and forests (16.5%). China demonstrates a notably higher  
 410 reliance on forested areas for wind turbine siting compared to global patterns,  
 411 particularly in its southern provinces (Figure 9a11a), warranting careful ecological  
 412 assessment (Enevoldsen, 2016). In contrast, the United States distributes roughly half  
 413 (50%) of its wind turbines across croplands, supplemented by grassland deployments.  
 414 Germany displays the most extreme geographic specialization, with over 90% of its  
 415 wind turbines sited exclusively on agricultural lands. These pronounced regional  
 416 variations in wind turbine siting patterns carry significant implications for both  
 417 renewable energy development and landscape management policies.



418



419

420 **Figure 911.** Land use distribution of global onshore wind turbines. **(a)** Land use distribution of  
 421 global onshore wind turbines. **(b)** Land use area statistics occupied by onshore wind turbines  
 422 by country. **(c)** Percentages of difference in land use deployed by onshore wind turbines.

423 **3.5 Potential ~~dataset~~ applications of the dataset**

424 This open-access global onshore wind turbine dataset ([GonshoreWT2024](#)) could  
 425 establish a critical foundation for interdisciplinary research, facilitating integrated  
 426 studies in energy infrastructure planning, ecological impact evaluation, and land use  
 427 optimization. First, the geospatial wind turbine dataset enables rigorous biodiversity  
 428 impact assessments, including wildlife disturbance patterns and habitat fragmentation  
 429 analysis around wind energy installations (Bopucki and Perzanowski, 2018; McKay et  
 430 al., 2024). Particularly, studies have demonstrated that turbine blade rotation creates  
 431 distinct mortality patterns across bird and bat species (Marques et al., 2020; Millon et  
 432 al., 2018). Our precisely geolocated turbine records enable exact spatial correlation  
 433 between wind infrastructure and vulnerable species' high-activity areas, facilitating  
 434 data-driven assessments of avian and chiropteran collision risks.

435 Second, wind farm construction and associated infrastructure development induce  
 436 significant ecological disruptions through multiple pathways (Xia et al., 2025).  
 437 Integrating high-precision turbine locations with remote sensing data allows systematic  
 438 evaluation of wind energy's environmental footprint, including deforestation patterns  
 439 (Enevoldsen, 2018), soil erosion (Ma et al., 2023), and carbon sink loss (Gao et al.,  
 440 2023). Our dataset provides a robust data foundation for both evaluating the cumulative  
 441 ecological impacts of existing wind farms and optimizing future turbine siting to

442 balance energy production with ecosystem conservation.

#### 443 **4 Data availability**

444 These open-access data resources could help promote transparent and just sustainable  
445 wind energy development, and enable detailed feature extraction and spatial analysis  
446 for future wind energy research. The global onshore wind turbine dataset  
447 ([GonshoreWT2024](#)) is freely available from the Zenodo website at:  
448 <https://doi.org/10.5281/zenodo.18984175>~~<https://doi.org/10.5281/zenodo.17217523>~~  
449 (Shujun et al., 2025).

450 The dataset includes:

451 ● A comprehensive global inventory of ~~416,532~~~~379,595~~ onshore wind turbines in the  
452 format of a geospatial shapefile. The dataset includes geolocation coordinates for  
453 all wind turbines, along with corresponding nation (Field: 'Nation') and land use  
454 classification (Field: 'landtype') for each wind turbine.

455 ~~● The dataset comprises 37,285 carefully annotated 256×256 pixel Google Earth~~  
456 ~~image patches, containing both positive (wind turbine) and negative (background)~~  
457 ~~samples, and is organized into folders with training (60%, 22,372 images) and~~  
458 ~~testing sets (20%, 7,457 images) validating sets (20%, 7,456 images). The images~~  
459 ~~could serve as foundational data for training deep learning models in wind turbine~~  
460 ~~classification, segmentation, and detection tasks.~~

461 ~~The~~The code file includes:

462 ● A PyTorch-based ResNet-18 implementation for classifying onshore wind turbines  
463 in Google Earth images, including codes for model architecture and pre-trained  
464 weights.

465 ● The GEE-based code for the Random Forest model, including sample point  
466 splitting (training/test sets) and model training.

#### 467 **5 Discussion and conclusion**

468 This study introduces an advanced geospatial approach that integrates high-resolution  
469 Google Earth images with multi-source satellite observations to construct a refined  
470 global inventory of onshore wind turbines. Compared to the current datasets of  
471 available global onshore wind turbines, our dataset provides more timely data that  
472 represents a tenfold expansion over the global wind turbine inventories as of 2020.  
473 Importantly, in mapping methodology, compared to the new updating framework of  
474 Global Renewables Watch, we propose a reproducible and straightforward approach to  
475 identify renewable infrastructure, which can be applied in future studies and in  
476 countries or regions with limited computational resources. The datasets and resulting  
477 2024 global inventory ~~documents~~~~document~~ ~~416,532~~~~379,595~~ onshore wind turbines,  
478 serving as a critical resource for renewable energy infrastructure planning and  
479 ecological impact studies.

480 The global analysis demonstrates significant spatial aggregation of wind turbines, with  
481 the densest concentrations occurring in northern mid-latitude zones, particularly high-  
482 density concentrations in Europe, North America, and East Asia. This spatial  
483 concentration pattern stems from factors including optimal wind resources (Davis et al.,  
484 2023; Liu et al., 2023), supportive policy frameworks (Godby et al., 2025; Kumar et al.,  
485 2022; Liao, 2016), and established energy infrastructure networks (Oró et al., 2015;  
486 Rochmińska, 2023) prevalent in these mid-latitude zones. Notably, the global wind  
487 energy has developed across 367,132,242,940 km<sup>2</sup> of land, with ~~agricultural fields~~  
488 croplands (4245%) and grasslands (3842%) hosting the majority (8087%) of turbine  
489 installations. This distribution reflects a strategic preference for siting turbines in  
490 previously developed or ecologically low-sensitivity areas. However, the associated  
491 ecological impacts, particularly habitat fragmentation and soil disturbance, require  
492 thorough environmental evaluation and mitigation planning (Moore O'Leary et al.,  
493 2017).

494 Wind turbines primarily appear as point features in satellite images, presenting  
495 significant challenges for automated large-scale detection (Zhai et al., 2024). These  
496 detection challenges are further intensified by visually similar infrastructure,  
497 particularly high-voltage transmission lines and isolated structures that mimic turbine  
498 signatures. Our proposed solution combines hybrid machine/deep learning  
499 architectures with systematic sampling approaches to enable reliable turbine  
500 identification across diverse terrain types. Looking ahead, sustainable renewable energy  
501 development, including wind, solar, and hydropower, requires continuous innovation  
502 and open geospatial data to enhance planning transparency and governance. Overall,  
503 our framework offers a novel approach and solution for cost-effective, timely updates  
504 of global onshore wind turbine data.

505 **Author contributions.** SL and PW designed the study and wrote the original  
506 manuscript. SL designed the methods and carried out the experiments and validation.  
507 JQ and YS edited and revised the paper.

508 **Competing interests.** The contact author has declared that none of the authors has any  
509 competing interests.

510 **Disclaimer.** Publisher's note: Copernicus Publications remains neutral with regard to  
511 jurisdictional claims in published maps and institutional affiliations.

512 **Acknowledgements.** The authors are grateful to the ESA's Copernicus program for  
513 providing free access to the Sentinel-1/2 data and the Google Earth Engine platform for  
514 preprocessing and making the data accessible. We also thank ~~the~~ OpenStreetMap for  
515 providing global onshore wind turbine locations and the land polygon data.

516 **Financial support.** This work was supported by the National Key Research and  
517 Development Program (Grant No.2023YFC3904500).

518

## 519 **References**

520 ~~Bopucki, R. and Perzanowski, K.: Effects of wind turbines on spatial distribution of the european hamster,~~

521 *Ecol. Indic.*, 84, 433–436, 2018.

522 Calvert, K., Pearce, J. M., and Mabee, W. E.: Toward renewable energy geo-information infrastructures:  
523 applications of giscience and remote sensing that build institutional capacity, *Renewable and Sustainable*  
524 *Energy Reviews*, 18, 416–429, 2013.

525 Cerri, J., Costantino, C., De Rosa, D., Banić, D. A., Urgeghe, G., Fozzi, I., Echeverria, J., Aresu, M., and  
526 Berlinguer, F.: Widely used datasets of wind energy infrastructures can seriously underestimate onshore  
527 turbines in the mediterranean, *Biol. Conserv.*, 300, 110870, 2024.

528 Congalton, R. G.: A review of assessing the accuracy of classifications of remotely sensed data, *Remote*  
529 *Sens. Environ.*, 37, 35–46, 1991.

530 Dai, T., Jose Valanarasu, J. M., Zhao, Y., Zheng, S., Sun, Y., Patel, V. M., and Jordaan, S. M.: Land  
531 resources for wind energy development requires regionalized characterizations, *Environ. Sci. Technol.*,  
532 58, 5014–5023, 2024.

533 Davis, N. N., Badger, J., Hahmann, A. N., Hansen, B. O., Mortensen, N. G., Kelly, M., Larsén, X. G.,  
534 Olsen, B. T., Floors, R., and Lizcano, G.: The global wind atlas: a high-resolution dataset of climatologies  
535 and associated web-based application, *Bull. Amer. Meteorol. Soc.*, 104, E1507–E1525, 2023.

536 Dunnett, S., Sorichetta, A., Taylor, G., and Eigenbrod, F.: Harmonised global datasets of wind and solar  
537 farm locations and power, *Sci. Data*, 7, 130, 2020.

538 Effenberger, N. and Ludwig, N.: A collection and categorization of open – source wind and wind power  
539 datasets, *Wind Energy*, 25, 1659–1683, 2022.

540 Enevoldsen, P.: Onshore wind energy in northern european forests: reviewing the risks, *Renewable and*  
541 *Sustainable Energy Reviews*, 60, 1251–1262, 2016.

542 Enevoldsen, P.: A socio-technical framework for examining the consequences of deforestation: a case  
543 study of wind project development in northern europe, *Energy Policy*, 115, 138–147, 2018.

544 Gao, L., Wu, Q., Qiu, J., Mei, Y., Yao, Y., Meng, L., and Liu, P.: The impact of wind energy on plant  
545 biomass production in china, *Sci. Rep.*, 13, 22366, 2023.

546 Godby, R., Cook, B., Holland, M., and Kjørstad, T.: State incentives: impact on wind energy costs and  
547 policy development, *Renewable and Sustainable Energy Reviews*, 215, 115572, 2025.

548 Goutte, C. and Gaussier, E.: A probabilistic interpretation of precision, recall and f score, with  
549 implication for evaluation, in: *European conference on information retrieval*, Springer, 345–359, 2005.

550 He, K., Zhang, X., Ren, S., and Sun, J.: Deep residual learning for image recognition, in: *Proceedings of*  
551 *the IEEE conference on computer vision and pattern recognition*, IEEE, Las Vegas, NV, USA, 770–778,  
552 2016.

553 Hoerer, T., Feuerstein, S., and Kuenzer, C.: Deepowl: a global offshore wind turbine data set derived  
554 with deep learning from sentinel-1 data, *Earth System Science Data Discussions*, 2022, 1–26, 2022.

555 Huang, S., Tang, L., Hupy, J. P., Wang, Y., and Shao, G.: A commentary review on the use of normalized  
556 difference vegetation index (ndvi) in the era of popular remote sensing, *J. For. Res.*, 32, 1–6, 2021.

557 Karra, K., Kontgis, C., Statman-Weil, Z., Mazzariello, J. C., Mathis, M., and Brumby, S. P.: Global land  
558 use/land cover with sentinel 2 and deep learning, in: *2021 IEEE international geoscience and remote*  
559 *sensing symposium IGARSS*, IEEE, Brussels, Belgium, 4704–4707, 2021.

560 Kati, V., Kassara, C., Vrontisi, Z., and Moustakas, A.: The biodiversity-wind energy-land use nexus in a  
561 global biodiversity hotspot, *Sci. Total Environ.*, 768, 144471, 2021.

562 Kleebauer, M., Karamanski, S., Callies, D., and Braun, M.: A wind turbines dataset for south africa:  
563 openstreetmap data, deep-learning-based geo-coordinate correction and capacity analysis, *Isprs Int. J.*  
564 *Geo-Inf.*, 14, 232, 2025.

565 Kruitwagen, L., Story, K. T., Friedrich, J., Byers, L., Skillman, S., and Hepburn, C.: A global inventory  
566 of photovoltaic solar energy generating units, *Nature*, 598, 604–610, 2021.

567 Kumar, A., Pal, D., Kar, S. K., Mishra, S. K., and Bansal, R.: An overview of wind energy development  
568 and policy initiatives in india, *Clean Technol. Environ. Policy*, 24, 1337–1358, 2022.

569 Liao, Z.: The evolution of wind energy policies in china (1995–2014): an analysis based on policy  
570 instruments, *Renewable and Sustainable Energy Reviews*, 56, 464–472, 2016.

571 Liu, Y., Feng, S., Qian, Y., Huang, H., and Berg, L. K.: How do north-american weather regimes drive  
572 wind energy at the sub-seasonal to seasonal timescales? *Npj Clim. Atmos. Sci.*, 6, 100, 2023.

573 Ma, B., Yang, J., Chen, X., Zhang, L., and Zeng, W.: Revealing the ecological impact of low-speed  
574 mountain wind power on vegetation and soil erosion in south china: a case study of a typical wind farm  
575 in yunnan, *J. Clean. Prod.*, 419, 138020, 2023.

576 Manske, D., Grosch, L., Schmiedt, J., Mittelstädt, N., and Thrän, D.: Geo-locations and system data of  
577 renewable energy installations in germany, *Data*, 7, 128, 2022.

578 Marques, A. T., Santos, C. D., Hanssen, F., Muñoz, A. R., Onrubia, A., Wikelski, M., Moreira, F.,  
579 Palmeirim, J. M., and Silva, J. P.: Wind turbines cause functional habitat loss for migratory soaring birds,  
580 *J. Anim. Ecol.*, 89, 93–103, 2020.

581 McKay, R. A., Johns, S. E., Bischof, R., Matthews, F., van der Kooij, J., Yoh, N., and Eldegard, K.: Wind  
582 energy development can lead to guild-specific habitat loss in boreal forest bats, *Wildlife Biol.*, 2024,  
583 e1168, 2024.

584 McKenna, R., Lilliestam, J., Heinrichs, H. U., Weinand, J., Schmidt, J., Staffell, I., Hahmann, A. N.,  
585 Burgherr, P., Burdack, A., and Bucha, M.: System impacts of wind energy developments: key research  
586 challenges and opportunities, *Joule*, 9, 2025.

587 Millon, L., Colin, C., Brescia, F., and Kerbiriou, C.: Wind turbines impact bat activity, leading to high  
588 losses of habitat use in a biodiversity hotspot, *Ecol. Eng.*, 112, 51–54, 2018.

589 Mishra, M., Desul, S., Santos, C. A. G., Mishra, S. K., Kamal, A. H. M., Goswami, S., Kalumba, A. M.,  
590 Biswal, R., Da Silva, R. M., and Dos Santos, C. A. C.: A bibliometric analysis of sustainable development  
591 goals (sdgs): a review of progress, challenges, and opportunities, *Environment, Development and  
592 Sustainability*, 26, 11101–11143, 2024.

593 Moore O'Leary, K. A., Hernandez, R. R., Johnston, D. S., Abella, S. R., Tanner, K. E., Swanson, A. C.,  
594 Kreidler, J., and Lovich, J. E.: Sustainability of utility-scale solar energy—critical ecological concepts,  
595 *Front. Ecol. Environ.*, 15, 385–394, 2017.

596 Muller, E., Gremmo, S., Houtin-Mongrolle, F., Duboc, B., and Bénard, P.: Field data-based validation  
597 of an aero-servo-elastic solver for high-fidelity large-eddy simulations of industrial wind turbines, *Wind  
598 Energy Sci.*, 9, 25–48, 2024.

599 Oró, E., Depoorter, V., Garcia, A., and Salom, J.: Energy efficiency and renewable energy integration in  
600 data centres. Strategies and modelling review, *Renewable and Sustainable Energy Reviews*, 42, 429–445,  
601 2015.

602 Raimi, D., Zhu, Y., Newell, R. G., Prest, B. C., and Bergman, A.: Global energy outlook 2023: sowing  
603 the seeds of an energy transition, *Resour. Future*, 1, 1–44, 2023.

604 Rand, J. T., Kramer, L. A., Garrity, C. P., Hoen, B. D., Diffendorfer, J. E., Hunt, H. E., and Spears, M.:  
605 A continuously updated, geospatially rectified database of utility-scale wind turbines in the united states,  
606 *Sci. Data*, 7, 15, 2020.

607 Rigatti, S. J.: Random forest, *Journal of Insurance Medicine*, 47, 31–39, 2017.

608 Rinne, E., Holttinen, H., Kiviluoma, J., and Rissanen, S.: Effects of turbine technology and land use on

609 [wind power resource potential, Nat. Energy, 3, 494-500, 2018.](#)  
610 [Robinson, C., Ortiz, A., Kim, A., Dodhia, R., Zolli, A., Nagaraju, S. K., Oakleaf, J., Kiesecker, J., and](#)  
611 [Ferre, J. M. L.: Global renewables watch: a temporal dataset of solar and wind energy derived from](#)  
612 [satellite imagery, Arxiv Preprint Arxiv:2503.14860, 2025.](#)  
613 [Rochmińska, A.: Wind energy infrastructure and socio-spatial conflicts, Energies, 16, 1032, 2023.](#)  
614 [Roddis, P., Carver, S., Dallimer, M., Norman, P., and Ziv, G.: The role of community acceptance in](#)  
615 [planning outcomes for onshore wind and solar farms: an energy justice analysis, Appl. Energy, 226, 353-](#)  
616 [364, 2018.](#)  
617 [Shujun, L., Jianchuan, Q., Yongze, S., and Wang, P.: Mapping global onshore wind turbines using multi-](#)  
618 [source remote sensing images and hybrid learning approaches, 2025.](#)  
619 [Smeraldo, S., Bosso, L., Fraissinet, M., Bordignon, L., Brunelli, M., Ancillotto, L., and Russo, D.:](#)  
620 [Modelling risks posed by wind turbines and power lines to soaring birds: the black stork \(\*Ciconia nigra\*\)](#)  
621 [in Italy as a case study, Biodivers. Conserv., 29, 1959-1976, 2020.](#)  
622 [Tavakkoli, S., Macknick, J., Heath, G. A., and Jordaan, S. M.: Spatiotemporal energy infrastructure](#)  
623 [datasets for the United States: a review, Renewable and Sustainable Energy Reviews, 152, 111616, 2021.](#)  
624 [Xia, Z., Li, Y., Guo, S., Zhang, X., Pan, X., Fang, H., Chen, R., and Du, P.: Assessment of forest](#)  
625 [disturbance and soil erosion in wind farm project using satellite observations, Resources, Conservation](#)  
626 [and Recycling, 212, 107934, 2025.](#)  
627 [Zha, Y., Gao, J., and Ni, S.: Use of normalized difference built-up index in automatically mapping urban](#)  
628 [areas from TM imagery, Int. J. Remote Sens., 24, 583-594, 2003.](#)  
629 [Zhai, Y., Chen, X., Cao, X., and Cui, X.: Identifying wind turbines from multiresolution and](#)  
630 [multibackground remote sensing imagery, Int. J. Appl. Earth Obs. Geoinf., 126, 103613, 2024.](#)  
631 [Zhang, T., Tian, B., Sengupta, D., Zhang, L., and Si, Y.: Global offshore wind turbine dataset, Sci. Data,](#)  
632 [8, 191, 2021.](#)

633

## 634 **References**

635 [Bopucki, R. and Perzanowski, K.: Effects of wind turbines on spatial distribution of the European](#)  
636 [hamster, Ecol. Indic., 84, 433-436, 2018.](#)  
637 [Calvert, K., Pearce, J. M., and Mabee, W. E.: Toward renewable energy geo-information infrastructures:](#)  
638 [applications of GIScience and remote sensing that build institutional capacity, Renewable and Sustainable](#)  
639 [Energy Reviews, 18, 416-429, 2013.](#)  
640 [Cerri, J., Costantino, C., De Rosa, D., Banič, D. A., Urgeghe, G., Fozzi, I., Echeverria, J., Aresu, M., and](#)  
641 [Berlinguer, F.: Widely used datasets of wind energy infrastructures can seriously underestimate onshore](#)  
642 [turbines in the Mediterranean, Biol. Conserv., 300, 110870, 2024.](#)  
643 [Congalton, R. G.: A review of assessing the accuracy of classifications of remotely sensed data, Remote](#)  
644 [Sens. Environ., 37, 35-46, 1991.](#)  
645 [Dai, T., Jose Valanarasu, J. M., Zhao, Y., Zheng, S., Sun, Y., Patel, V. M., and Jordaan, S. M.: Land](#)  
646 [resources for wind energy development require regionalized characterizations, Environ. Sci. Technol.,](#)  
647 [58, 5014-5023, 2024.](#)  
648 [Davis, N. N., Badger, J., Hahmann, A. N., Hansen, B. O., Mortensen, N. G., Kelly, M., Larsén, X. G.,](#)  
649 [Olsen, B. T., Floors, R., and Lizcano, G.: The global wind atlas: a high-resolution dataset of climatologies](#)  
650 [and associated web-based application, Bull. Amer. Meteorol. Soc., 104, E1507-E1525, 2023.](#)  
651 [Dunnett, S., Sorichetta, A., Taylor, G., and Eigenbrod, F.: Harmonised global datasets of wind and solar](#)  
652 [farm locations and power, Sci. Data, 7, 130, 2020.](#)

653 [Effenberger, N. and Ludwig, N.: A collection and categorization of open - source wind and wind power](#)  
654 [datasets, Wind Energy, 25, 1659-1683, 2022.](#)

655 [Enevoldsen, P.: Onshore wind energy in northern European forests: reviewing the risks, Renewable and](#)  
656 [Sustainable Energy Reviews, 60, 1251-1262, 2016.](#)

657 [Enevoldsen, P.: A socio-technical framework for examining the consequences of deforestation: a case](#)  
658 [study of wind project development in northern Europe, Energy Policy, 115, 138-147, 2018.](#)

659 [Gao, L., Wu, Q., Qiu, J., Mei, Y., Yao, Y., Meng, L., and Liu, P.: The impact of wind energy on plant](#)  
660 [biomass production in China, Sci. Rep., 13, 22366, 2023.](#)

661 [Godby, R., Cook, B., Holland, M., and Kjorstad, T.: State incentives: impact on wind energy costs and](#)  
662 [policy development, Renewable and Sustainable Energy Reviews, 215, 115572, 2025.](#)

663 [Goutte, C. and Gaussier, E.: A probabilistic interpretation of precision, recall and f-score, with](#)  
664 [implications for evaluation, in: European Conference on Information Retrieval, Springer, 345-359, 2005.](#)

665 [He, K., Zhang, X., Ren, S., and Sun, J.: Deep residual learning for image recognition, in: Proceedings of](#)  
666 [the IEEE conference on computer vision and pattern recognition, IEEE, Las Vegas, NV, USA, 770-778,](#)  
667 [2016.](#)

668 [Hoeser, T., Feuerstein, S., and Kuenzer, C.: Deepowt: a global offshore wind turbine data set derived](#)  
669 [with deep learning from Sentinel-1 data, Earth System Science Data Discussions, 2022, 1-26, 2022.](#)

670 [Huang, S., Tang, L., Hupy, J. P., Wang, Y., and Shao, G.: A commentary review on the use of normalized](#)  
671 [difference vegetation index \(NDVI\) in the era of popular remote sensing, J. For. Res., 32, 1-6, 2021.](#)

672 [Karra, K., Kontgis, C., Statman-Weil, Z., Mazzariello, J. C., Mathis, M., and Brumby, S. P.: Global land](#)  
673 [use/land cover with Sentinel-2 and deep learning, in: 2021 IEEE International Geoscience and Remote](#)  
674 [Sensing Symposium IGARSS, IEEE, Brussels, Belgium, 4704-4707, 2021.](#)

675 [Kati, V., Kassara, C., Vrontisi, Z., and Moustakas, A.: The biodiversity-wind energy-land use nexus in a](#)  
676 [global biodiversity hotspot, Sci. Total Environ., 768, 144471, 2021.](#)

677 [Kleebauer, M., Karamanski, S., Callies, D., and Braun, M.: A wind turbines dataset for South Africa:](#)  
678 [OpenStreetMap data, deep learning based geo-coordinate correction and capacity analysis, Isprs Int. J.](#)  
679 [Geo-Inf., 14, 232, 2025.](#)

680 [Kruitwagen, L., Story, K. T., Friedrich, J., Byers, L., Skillman, S., and Hepburn, C.: A global inventory](#)  
681 [of photovoltaic solar energy generating units, Nature, 598, 604-610, 2021.](#)

682 [Kumar, A., Pal, D., Kar, S. K., Mishra, S. K., and Bansal, R.: An overview of wind energy development](#)  
683 [and policy initiatives in India, Clean Technol. Environ. Policy, 24, 1337-1358, 2022.](#)

684 [Liao, Z.: The evolution of wind energy policies in China \(1995 - 2014\): an analysis based on policy](#)  
685 [instruments, Renewable and Sustainable Energy Reviews, 56, 464-472, 2016.](#)

686 [Liu, Y., Feng, S., Qian, Y., Huang, H., and Berg, L. K.: How do North American weather regimes drive](#)  
687 [wind energy at the sub-seasonal to seasonal timescales? Npj Clim. Atmos. Sci., 6, 100, 2023.](#)

688 [Ma, B., Yang, J., Chen, X., Zhang, L., and Zeng, W.: Revealing the ecological impact of low-speed](#)  
689 [mountain wind power on vegetation and soil erosion in South China: a case study of a typical wind farm](#)  
690 [in Yunnan, J. Clean. Prod., 419, 138020, 2023.](#)

691 [Manske, D., Grosch, L., Schmiedt, J., Mittelstädt, N., and Thrän, D.: Geo-locations and system data of](#)  
692 [renewable energy installations in Germany, Data, 7, 128, 2022.](#)

693 [Marques, A. T., Santos, C. D., Hanssen, F., Muñoz, A. R., Onrubia, A., Wikelski, M., Moreira, F.,](#)  
694 [Palmeirim, J. M., and Silva, J. P.: Wind turbines cause functional habitat loss for migratory soaring birds,](#)  
695 [J. Anim. Ecol., 89, 93-103, 2020.](#)

696 [Mckay, R. A., Johns, S. E., Bischof, R., Matthews, F., van der Kooij, J., Yoh, N., and Eldegard, K.: Wind](#)

697 [energy development can lead to guild - specific habitat loss in boreal forest bats, \*Wildlife Biol.\*, 2024,](#)  
698 [e1168, 2024.](#)

699 [Mckenna, R., Lilliestam, J., Heinrichs, H. U., Weinand, J., Schmidt, J., Staffell, I., Hahmann, A. N.,](#)  
700 [Burgherr, P., Burdack, A., and Bucha, M.: System impacts of wind energy developments: key research](#)  
701 [challenges and opportunities, \*Joule\*, 9, 2025.](#)

702 [Millon, L., Colin, C., Brescia, F., and Kerbirou, C.: Wind turbines impact bat activity, leading to high](#)  
703 [losses of habitat use in a biodiversity hotspot, \*Ecol. Eng.\*, 112, 51-54, 2018.](#)

704 [Mishra, M., Desul, S., Santos, C. A. G., Mishra, S. K., Kamal, A. H. M., Goswami, S., Kalumba, A. M.,](#)  
705 [Biswal, R., Da Silva, R. M., and Dos Santos, C. A. C.: A bibliometric analysis of sustainable development](#)  
706 [goals \(sdgs\): a review of progress, challenges, and opportunities, \*Environment, Development and\*](#)  
707 [Sustainability, 26, 11101-11143, 2024.](#)

708 [Moore O'Leary, K. A., Hernandez, R. R., Johnston, D. S., Abella, S. R., Tanner, K. E., Swanson, A. C.,](#)  
709 [Kreitler, J., and Lovich, J. E.: Sustainability of utility - scale solar energy - critical ecological concepts,](#)  
710 [Front. Ecol. Environ., 15, 385-394, 2017.](#)

711 [Muller, E., Gremmo, S., Houtin-Mongrolle, F., Duboc, B., and Bénard, P.: Field-data-based validation](#)  
712 [of an aero-servo-elastic solver for high-fidelity large-eddy simulations of industrial wind turbines, \*Wind\*](#)  
713 [Energy Sci., 9, 25-48, 2024.](#)

714 [Oró, E., Depoorter, V., Garcia, A., and Salom, J.: Energy efficiency and renewable energy integration in](#)  
715 [data centres. Strategies and modelling review, \*Renewable and Sustainable Energy Reviews\*, 42, 429-445,](#)  
716 [2015.](#)

717 [Raimi, D., Zhu, Y., Newell, R. G., Prest, B. C., and Bergman, A.: Global energy outlook 2023: sowing](#)  
718 [the seeds of an energy transition, \*Resour. Future\*, 1, 1-44, 2023.](#)

719 [Rand, J. T., Kramer, L. A., Garrity, C. P., Hoen, B. D., Diffendorfer, J. E., Hunt, H. E., and Spears, M.:](#)  
720 [A continuously updated, geospatially rectified database of utility-scale wind turbines in the United States,](#)  
721 [Sci. Data, 7, 15, 2020.](#)

722 [Rigatti, S. J.: Random Forest, \*Journal of Insurance Medicine\*, 47, 31-39, 2017.](#)

723 [Rinne, E., Holttinen, H., Kiviluoma, J., and Rissanen, S.: Effects of turbine technology and land use on](#)  
724 [wind power resource potential, \*Nat. Energy\*, 3, 494-500, 2018.](#)

725 [Robinson, C., Ortiz, A., Kim, A., Dodhia, R., Zolli, A., Nagaraju, S. K., Oakleaf, J., Kiesecker, J., and](#)  
726 [Ferres, J. M. L.: Global renewables watch: a temporal dataset of solar and wind energy derived from](#)  
727 [satellite imagery, Arxiv Preprint Arxiv:2503.14860, 2025.](#)

728 [Rochmińska, A.: Wind energy infrastructure and socio-spatial conflicts, \*Energies\*, 16, 1032, 2023.](#)

729 [Roddis, P., Carver, S., Dallimer, M., Norman, P., and Ziv, G.: The role of community acceptance in](#)  
730 [planning outcomes for onshore wind and solar farms: an energy justice analysis, \*Appl. Energy\*, 226, 353-](#)  
731 [364, 2018.](#)

732 [Shujun, L., Jianchuan, Q., Yongze, S., and Wang, P.: Mapping global onshore wind turbines using multi-](#)  
733 [source remote sensing images and hybrid learning approaches, 2025.](#)

734 [Smeraldo, S., Bosso, L., Fraissinet, M., Bordignon, L., Brunelli, M., Ancillotto, L., and Russo, D.:](#)  
735 [Modelling risks posed by wind turbines and power lines to soaring birds: the black stork \(\*Ciconia Nigra\*\)](#)  
736 [in Italy as a case study, \*Biodivers. Conserv.\*, 29, 1959-1976, 2020.](#)

737 [Tavakkoli, S., Macknick, J., Heath, G. A., and Jordaan, S. M.: Spatiotemporal energy infrastructure](#)  
738 [datasets for the United States: a review, \*Renewable and Sustainable Energy Reviews\*, 152, 111616, 2021.](#)

739 [Xia, Z., Li, Y., Guo, S., Zhang, X., Pan, X., Fang, H., Chen, R., and Du, P.: Assessment of forest](#)  
740 [disturbance and soil erosion in wind farm project using satellite observations, \*Resources, Conservation\*](#)

741 [and Recycling, 212, 107934, 2025.](#)

742 [Zha, Y., Gao, J., and Ni, S.: Use of normalized difference built-up index in automatically mapping urban](#)

743 [areas from tm imagery, Int. J. Remote Sens., 24, 583-594, 2003.](#)

744 [Zhai, Y., Chen, X., Cao, X., and Cui, X.: Identifying wind turbines from multiresolution and](#)

745 [multibackground remote sensing imagery, Int. J. Appl. Earth Obs. Geoinf., 126, 103613, 2024.](#)

746 [Zhang, T., Tian, B., Sengupta, D., Zhang, L., and Si, Y.: Global offshore wind turbine dataset, Sci. Data,](#)

747 [8, 191, 2021.](#)

748